scientific reports

Check for updates

OPEN

Robust skyrmion mediated reversal of ferromagnetic nanodots of 20 nm lateral dimension with high M_s and observable DMI

Md Mahadi Rajib[1], Walid Al Misba[1], Dhritiman Bhattacharya[1] & Jayasimha Atulasimha[1,2]✉

Implementation of skyrmion based energy efficient and high-density data storage devices requires aggressive scaling of skyrmion size. Ferrimagnetic materials are considered to be a suitable platform for this purpose due to their low saturation magnetization (i.e. smaller stray field). However, this method of lowering the saturation magnetization and scaling the lateral size of skyrmions is only applicable where the skyrmions have a smaller lateral dimension compared to the hosting film. Here, we show by performing rigorous micromagnetic simulation that the size of skyrmions, which have lateral dimension comparable to their hosting nanodot can be scaled by increasing saturation magnetization. Also, when the lateral dimension of nanodot is reduced and thereby the skyrmion confined in it is downscaled, there remains a challenge in forming a stable skyrmion with experimentally observed Dzyaloshinskii–Moriya interaction (DMI) values since this interaction has to facilitate higher canting per spin to complete a 360° rotation along the diameter. In our study, we found that skyrmions can be formed in 20 nm lateral dimension nanodots with high saturation magnetization (1.30–1.70 MA/m) and DMI values (~ 3 mJ/m^2) that have been reported to date. This result could stimulate experiments on implementation of highly dense skyrmion devices. Additionally, using this, we show that voltage controlled magnetic anisotropy based switching mediated by an intermediate skyrmion state can be achieved in the soft layer of a ferromagnetic p-MTJ of lateral dimensions 20 nm with sub 1 fJ/bit energy in the presence of room temperature thermal noise with reasonable DMI ~ 3 mJ/m^2.

Skyrmions are particle-like localized spin structures which can potentially overcome pinning with much smaller currents compared to domain walls (DW)[1–7]. This characteristic provides a pathway to implement energy efficient racetrack devices[7–10]. Skyrmions confined in the free layer of a Magnetic Tunnel Junction (MTJ) switched by electrical fields can also function as memory devices[11,12]. For example, skyrmions can assist voltage controlled magnetic anisotropy (VCMA) switching of perpendicular ferromagnets from up/down state to down/up state acting as an intermediate state[13–15]. This skyrmion mediated VCMA reversal has been shown to be robust while not requiring a bias magnetic field[13]. This could lead to scalable and energy efficient (< 1fJ/bit) VCMA switched MTJs [13,15,16]. However, aggressive scaling of skyrmion size, both in racetrack and MTJ devices, is required to make them competitive with existing spin-transfer torque magnetic random-access memory (STT-MRAM) devices in terms of density and energy efficiency.

Multilayer thin ferromagnetic film stacks have been optimized to reduce skyrmion size down to ~ 30 nm starting from several micrometer lateral dimensions at room temperature[17–20]. Unfortunately, large stray fields originating from ferromagnets impede further scaling of skyrmions in thin films[21]. In confined structures, it has been previously shown that creation, annihilation and dynamics of skyrmions is drastically different from thin films due to the influence of geometric boundary on skyrmion stability and dynamics[6,22,23]. Though there have been few studies on skyrmions in a confined structure[24–27], no prior work studied the requirement of both saturation magnetization (M_s) and Dzyaloshinskii–Moriya Interaction (DMI) as the lateral dimension is down-scaled to very small sizes ~ 20 nm. We previously showed ferromagnetic skyrmions cannot be formed in a 20 nm nanodot with experimentally observed DMI (~ 3.3 mJ/m^2[28]) and require extremely large DMI (~ 13 mJ/m^2)[15].

[1]Department of Mechanical and Nuclear Engineering, Virginia Commonwealth University, Richmond, VA 23284, USA. [2]Department of Electrical and Computer Engineering, Virginia Commonwealth University, Richmond, VA 23284, USA. ✉email: jatulasimha@vcu.edu

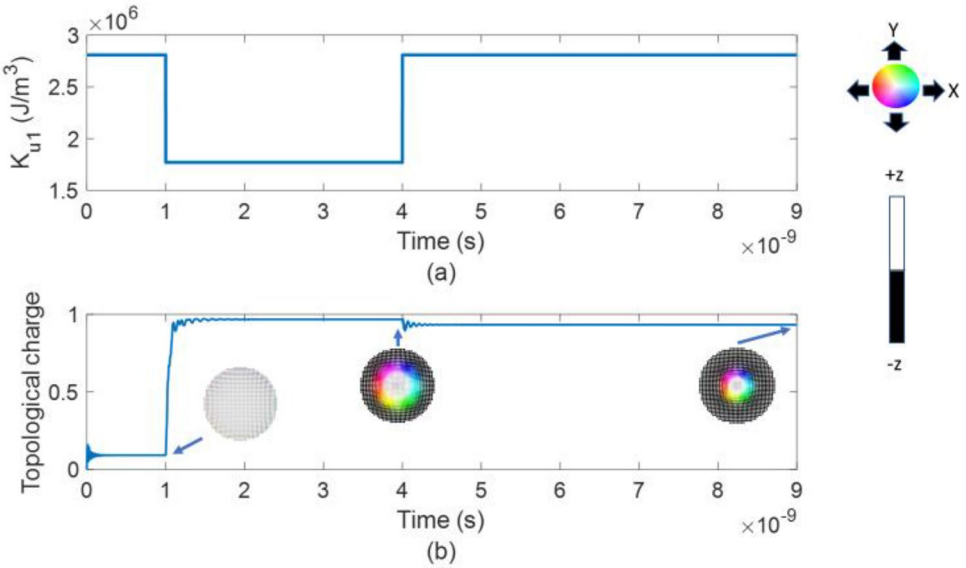

Figure 1. (**a**) Application of VCMA, (**b**) A quasi-ferromagnetic (QFM) state is created after relaxing for 1 ns. After the reduction of PMA, a skyrmion is formed and it is stable even after the withdrawal of voltage pulse.

Hence, compensated ferrimagnets have recently emerged as an alternative to ferromagnets for hosting smaller skyrmions due to their small stray fields[29,30]. Skyrmion as small as ~ 10 nm has been observed in ferrimagnetic thin film of $Co_{56}Gd_{44}$ at room temperature[29]. However, in this work we show that high saturation magnetization favors formation of skyrmions in confined structures of small lateral dimensions (e.g. nanodots ~ 20 nm) as opposed to the case of ferrimagnetic thin films where weak stray fields due to low net saturation magnetization helps form smaller skyrmions. We also show that thermally robust skyrmion mediated switching can be attained in a 20 nm nanodot with high saturation magnetization and DMI values ~ 3 mJ/m^2; both material parameters have been experimentally realized[28,31,32].

Results and discussion

Formation of skyrmion in smaller nanodots requires higher M_s and DMI (simulations at 0 K). To study the formation of a stable skyrmion we simulated the magnetization dynamics of circular nanodots of 50 nm, 30 nm and 20 nm diameter in response to an applied voltage pulse as shown in Fig. 1a using the micromagnetic simulation software Mumax3[33]. In all three cases, we initiate the simulations from a purely ferromagnetic state (all the spins pointing in the + z direction) and relax for 1 ns which ends up as a quasi-ferromagnet (QFM) state as shown in Fig. 1b. We can see that in a QFM state the boundary spins are slightly tilted. The perpendicular magnetic anisotropy (PMA) is then reduced through VCMA in 0.5 ps (see Supplementary Information section 1). After 3 ns, the voltage pulse is withdrawn and the PMA is restored to the initial value as shown in Fig. 1a. We see the equilibrium state after 5 ns and observe that the final state is either a QFM or a skyrmion. We find that after the withdrawal of voltage pulse, 5 ns is sufficient for reaching a stable state. This was confirmed by studying one equilibrium state (M_s = 1650 kA/m, DMI = 3.2 mJ/m^2) for 1 μs and there was no change in average out-of-plane magnetization component or topological charge from those obtained after 5 ns. To find the required saturation magnetization (M_s) and DMI as the lateral dimension of the nanodot is varied, the initial and reduced effective perpendicular anisotropy energy along with other parameters listed in Table 1 of the method section are kept constant. The effective PMA energy is expressed as $K_{eff}\,V = \left(K_{u1} - \frac{1}{2}\mu_0 M_s^2\right)V$, where K_{eff} is the effective PMA energy density, K_{u1} is the PMA constant (uniaxial anisotropy) and V is the volume of the nanodot. The saturation magnetization is varied from 700 kA/m to 1700 kA/m for all nanodots.

The stable state turns out to be either a QFM or a skyrmion state. Figure 1 shows an example case of formation of a stable skyrmion in a 20 nm nanodot through VCMA where M_s = 1650 kA/m and DMI = 3.2 mJ/m^2. The skyrmion is created when the effective PMA energy is reduced and remains stable even after the restoration of effective PMA energy to the initial value by withdrawing the voltage pulse.

By following the strategy illustrated in Fig. 1a we observe the required M_s and DMI values for which skyrmions are formed in 20 nm, 30 nm and 50 nm nanodots. This is shown by DMI-M_s phase diagrams in Fig. 2.

It is understandable that in a 20 nm nanodot there will be higher tilting per spin to complete a 360° rotation along the diameter and the requirement of DMI will be higher compared to 30 nm and 50 nm nanodot for a constant effective PMA energy. Previously it has been shown that even for formation of transient skyrmion in a 20 nm nanodot, an extremely large DMI (~ 13 mJ/m^2) is required[15]. So, it becomes a challenge to create a skyrmion in a 20 nm nanodot with experimentally observed DMI. Therefore, we focus on exploring the minimum DMI value with which a stable skyrmion can be formed under a constant effective PMA energy while the DMI is within the observable limit. We also observe the required saturation magnetization associated with the minimum DMI to explore which minimum DMI and M_s combination helps stabilize skyrmions in the nanodots. In

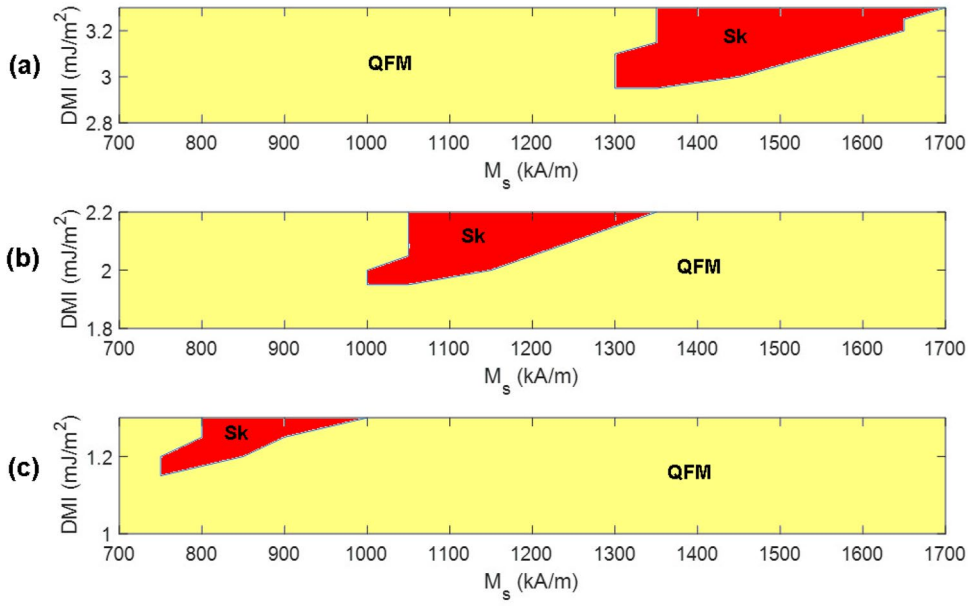

Figure 2. DMI-M_s phase diagram for (**a**) 20 nm, (**b**) 30 nm and (**c**) 50 nm (QFM and Sk in the phase diagrams represent the regions where quasi-ferromagnetic and skyrmion states are observed).

addition to that, we explore some other DMI values close to the minimum DMI and observe the corresponding M_s values for the formation of a skyrmion as shown in Fig. 2.

Figure 2a shows the DMI-M_s phase diagram for a 20 nm nanodot. We can see that minimum DMI for creating a stable skyrmion with a constant effective PMA energy as mentioned in Table 1 is 2.95 mJ/m^2. Saturation magnetization required to form the skyrmion at this DMI value is 1300–1350 kA/m. Below 2.95 mJ/m^2 DMI, no skyrmion is formed. As the DMI value is increased, the M_s range for which skyrmion can be created becomes wider on the higher end of M_s values. Considering a 1 nm thick MgO layer and an application of a voltage pulse of 2.0 V, the VCMA coefficient required to form these skyrmions in a 20 nm nanodot is 312 fJ/Vm[34], see Supplementary Information section 2.

We next increased the lateral dimension to 30 nm and explored the minimum DMI required to form skyrmions in the 700–1700 kA/m M_s range at the effective PMA energy equal to that of 20 nm. From Fig. 2b we can see that the required minimum DMI is 1.95 mJ/m^2 and the M_s is 1000–1050 kA/m for the formation of skyrmions in a 30 nm nanodot. At higher DMI, the M_s range for which the skyrmion is created grows wider on the higher end of M_s values similar to the 20 nm case.

The DMI-M_s relation required for formation of a stable skyrmion in increased lateral dimension nanodot of 50 nm is shown in Fig. 2c. Minimum DMI required for the formation of a stable skyrmion is 1.15 mJ/m^2 and corresponding M_s value is 750 kA/m. Considering the MgO layer thickness and application of voltage pulse are the same as 20 nm, the VCMA coefficients required for skyrmion formation in 30 nm and 50 nm nanodots are 139 fJ/Vm and 50fJ/Vm respectively.

For 50 nm, though a skyrmion is observed for a minimum DMI value of 1.15 mJ/m^2 and M_s value of 750 kA/m, no skyrmion is found if the DMI is kept constant at 1.15 mJ/m^2 and M_s is increased. For other DMI values which are close to the minimum DMI, the required M_s remains in the comparatively lower end of M_s values. For 20 nm, the minimum DMI occurs at high M_s values relative to the 30 nm and 50 nm lateral dimension cases. For other DMI values close to the minimum DMI, the required M_s values are also on the higher end of M_s range. Expectedly, minimum DMI and M_s values for 30 nm fall in between those values required for 20 nm and 50 nm. Since the minimum DMI is associated with high M_s for 20 nm nanodots, we can say that large saturation magnetization helps stabilize skyrmions in smaller nanodots. This trend of downscaling of skyrmion lateral dimension draws a significant contrast with the downscaling of skyrmion size in thin films where lowering the saturation magnetization helps form smaller skyrmion. However, in nanodots, high saturation magnetization helps stabilize smaller skyrmions.

To study how the skyrmions are formed at high M_s in downscaled nanodots, we observe the dynamic evolution and total energy of the corresponding states for 20 nm nanodot for various M_s values. We take two M_s values, one from the higher end (1650 kA/m) and the other from lower end (1000 kA/m) of M_s range at a constant DMI (3.2 mJ/m^2) and observed the dynamic evolution of the magnetic states and their corresponding energy as shown in Fig. 3. For 1000 kA/m, skyrmion forms after 25 ps when PMA is reduced. The breathing of skyrmion is very fast and annihilates after ~ 100 ps at reduced PMA. After the annihilation of skyrmions, the nanodot stabilizes at QFM state. The stable QFM can be seen at 4 ns and this state has higher energy compared to the stable skyrmion formed with 1650 kA/m M_s at reduced PMA. When PMA is restored by withdrawing the voltage pulse, a stable ferromagnetic state is observed as shown at 9 ns in Fig. 3. For 1650 kA/m M_s, a skyrmion

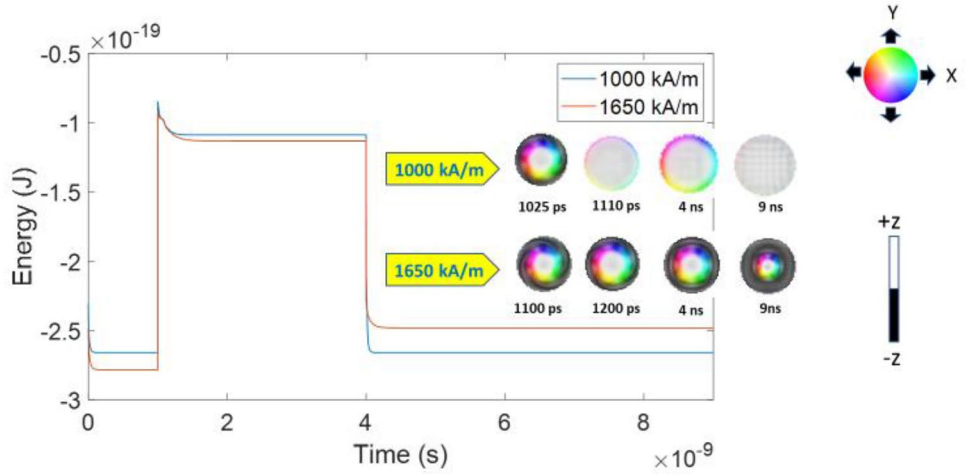

Figure 3. Evolution of total energy for two different M_s values and their corresponding magnetic states at different times.

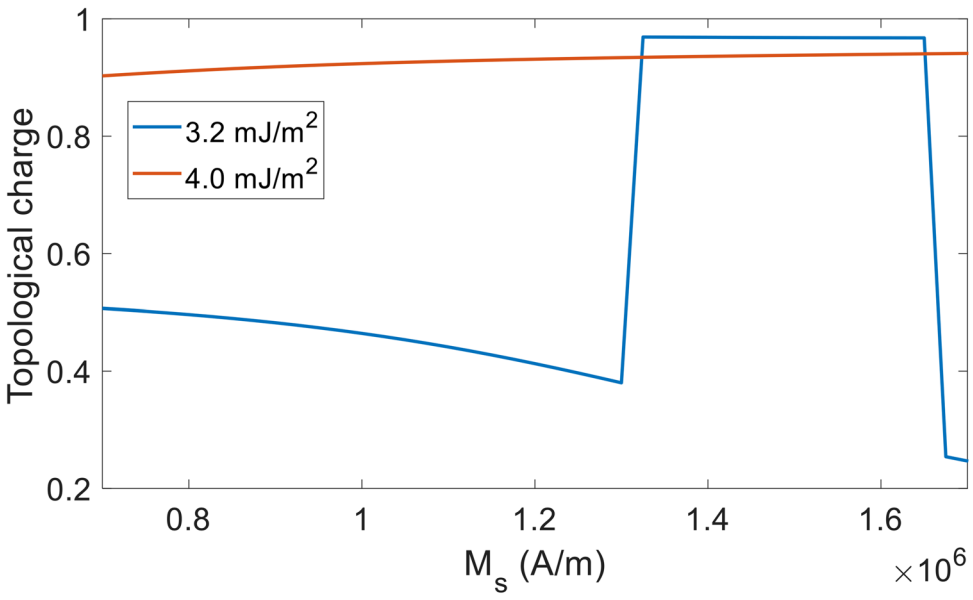

Figure 4. Topological charge vs. saturation magnetization of 20 nm nanodot for 3.2 mJ/m^2 and 4.0 mJ/m^2 DMI.

forms slowly, specifically ~ 100 ps after the PMA is reduced. The skyrmion formed in this case also breathes slowly and stabilizes at this state.

The requirement of higher DMI for decreased dimension of nanodots can be explained as follows. A higher DMI strength is required for completing the 360-degree rotation along a smaller diameter. Furthermore, when DMI is kept at the minimum required, high M_s is needed as it helps the formation of stray field dominated skyrmions in the confined nanostructure. Figure 4 shows that for 20 nm nanodots and 3.2 mJ/m^2 DMI, the minimum M_s at which a skyrmion is formed is 1350 kA/m whereas the minimum M_s for the formation of skyrmion at 4.0 mJ/m^2 DMI is only 700 kA/m. In summary, high M_s is not needed if we could employ high DMI and therefore form DMI mediated skyrmions. On the other hand, using low DMI requires a high M_s so that the stray field can aid the DMI in formation and stabilization of the skyrmions.

Skyrmion-mediated voltage controlled switching of ~ 20 nm nanodot (with inclusion of room temperature thermal noise). In this section, we study the switching probability of 20 nm lateral dimension ferromagnetic nanodot by employing VCMA induced skyrmion mediated switching. In such switching, an intermediate skyrmion is created starting from a ferromagnetic state by lowering PMA, which is subsequently annihilated by restoring the PMA to achieve switching from ferromagnetic up/down to down/up state (Fig. 5a). This reversal mechanism is implemented in a similar way that is followed for stabilizing skyrmions but the only

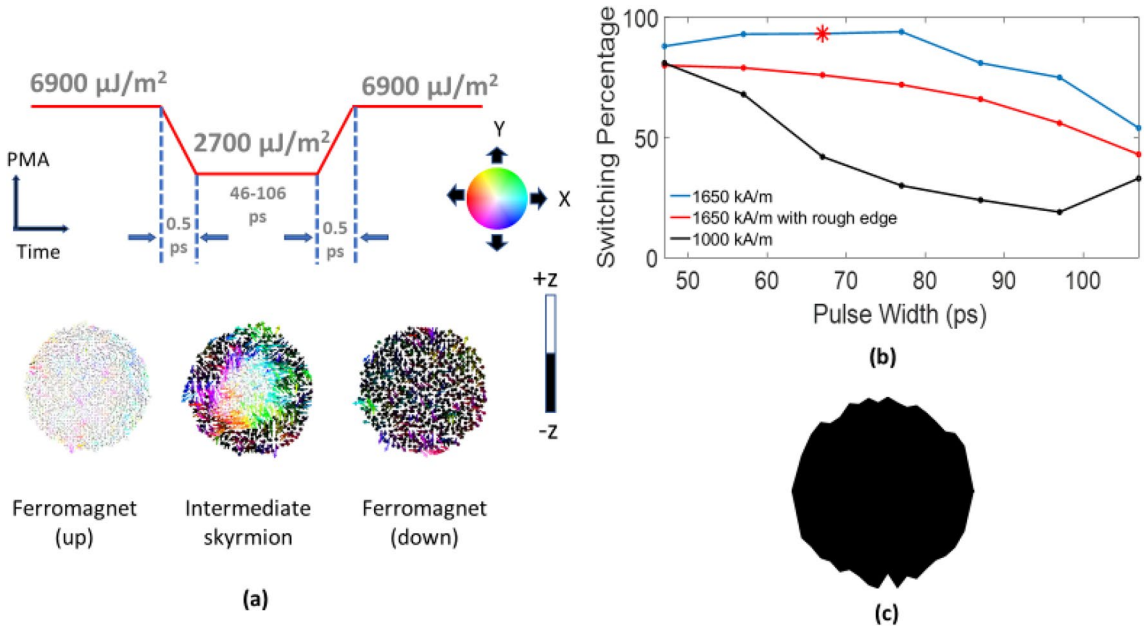

Figure 5. (**a**) Voltage pulse described in terms of PMA for switching of 20 nm nanodot in the presence of thermal perturbation; magnetization states corresponding to the PMA energy at different times are shown below the pulse diagram. (**b**) Switching percentage vs. pulse width (all of the points show the switching percentage for 100 simulation cases except the point marked with asterisk on the blue line. The star mark corresponds to a 67 ps pulse width where the simulations were run for 1000 times and 68 failures indicate ~ 93% switching) and (**c**) 20 nm nanodot with 5% edge roughness at the boundary.

Exchange stiffness	5 pJ/m[38]
Thickness	0.6 nm
Gilbert damping coefficient	0.05[39]
Cell size	0.5 nm × 0.5 nm × 0.6 nm
Initial effective PMA energy	1.30 eV
Reduced effective PMA energy	0.07 eV

Table 1. List of parameters.

difference is in the timing of withdrawal of the voltage pulse. In stabilization, the voltage pulse is withdrawn after the skyrmion has been stabilized after some initial breathing at reduced PMA, whereas in reversal the voltage pulse is withdrawn while the skyrmion breathes. From stabilization in the absence of thermal noise, we have seen that for both cases of M_s, a skyrmion is formed. However, for lower value of M_s the breathing is very fast and the skyrmion thus formed cannot be stabilized. While skyrmion mediated magnetization reversal only requires a transient skyrmion, stabilization guides the choice of a skyrmion that breathes slowly, survives longer and provides potential robust switching.

For stabilization of skyrmions in the absence of thermal noise, the stability factor ($K_{eff}V/k_BT$) at reduced PMA is ~ 2.73. However, a larger stability factor is needed in the presence of thermal noise. So, the thickness of the 20 nm nanodot is increased from 0.6 to 1.5 nm to make the transient skyrmion thermally stable while keeping the reduced effective PMA energy density constant (60,000 J/m^3) the same as non-thermal cases. Apart from increasing the thickness of the nanodot, the initial effective PMA energy density is also increased to ensure a thermally stable ferromagnetic state. For studying the switching probability, we take two M_s values, 1000 kA/m and 1650 kA/m at a constant DMI 3.2 mJ/m^2. The initial and reduced effective PMA energy are 330 k_BT and 6.83 k_BT respectively for the systems with M_s of 1000 kA/m and 1650 kA/m system. Therefore, the initial and reduced interfacial magnetic anisotropy (K_i) for 1650 kA/m are 6900 μJ/m^2 and 2700 μJ/m^2 whereas the corresponding values for 1000 kA/m are 5300 μJ/m^2 and 1000 μJ/m^2 respectively. From non-thermal stabilization we observed that for both values of M_s, initially a skyrmion is formed but for low value of M_s (1000 kA/m) this skyrmion does not stabilize. Since during reversal a transient skyrmion suffices, both low and high values of M_s are supposed to provide reversal if the voltage pulse is withdrawn synchronously with the breathing of the skyrmion. Therefore, we consider these two values of M_s to study which M_s value better favors the thermally robust switching . We let both systems relax for 100 ps to get the equilibrium state before trying to switch the magnetization. Due to the large PMA, this state is very close to the ferromagnetic state with very small canting of peripheral spins because of the stray field. After relaxing, we apply VCMA to reduce the PMA within 0.5 ps and a skyrmion is formed. We

then restore the PMA by withdrawing the voltage pulse at different points (times in formation and dynamics of the skyrmion state) and observe switching. We note that Fig. 5a shows the switching from ferromagnet (up) to ferromagnet (down) state for $M_s = 1650$ kA/m and DMI = 3.2 mJ/m^2 and the switching from ferromagnet (down) to ferromagnet (up) is shown in the Supplementary Information section 3. In this switching event, sub 1 fJ energy is dissipated on application of a voltage pulse of 2.0 V with 2130 fJ/Vm VCMA coefficient for a 1.5-nm-thick free layer and a 1-nm-thick MgO layer with relative permittivity ~ 7. We note that a high VCMA coefficient is needed as we chose a high initial PMA to ensure $K_{eff}V/k_BT \sim 330$. If we choose a smaller $K_{eff}V/k_BT \sim 68$, which suffices for Random Access Memory (RAM), an interfacial PMA energy ~ 3500 μJ/m^2 and VCMA coefficient ~ 405 fJ/Vm would be sufficient for the 1650 kA/m M_s system. We also note that for $K_{eff}V/k_BT \sim 68$, those required values would be well within the experimentally demonstrated values of interfacial PMA energy ~ 4060 μJ/m^2[35] and VCMA coefficient ~ 1043 fJ/Vm[36]. From Fig. 5b we can see that for a pulsewidth range of 47–107 ps, highest switching percentage for 1000 kA/m is 81% at 47 ps pulsewidth whereas for 1650 kA/m M_s, ~ 93% switching can be achieved in 57–77 ps pulse width range. For both stabilization and thermal reversal of skyrmions, it appears that the boundary spins initiate the process of skyrmion formation whereas the edges of the circular nanodot are nearly smooth. So, we studied this system's behavior in a nanodot where edge roughness is present. Therefore, we incorporated 5% edge roughness as shown in Fig. 5c at the boundary of the 20 nm nanodot to study the switching error in the same pulse width range of 47-107 ps. We note that the 5% edge roughness was created using a Gaussian distribution. From Fig. 5c we can see that in the presence of edge roughness for 1650 kA/m M_s and 3.2 mJ/m^2 DMI, ~ 80% switching can be attained in the pulse width range of 47–57 ps. With better optimization of the material parameters (e.g. high M_s and experimentally observed DMI) and pulse shaping[37], which is beyond the scope of this paper, higher switching percentage can be attained with sub fJ energy for each switching event. For example, the point in Fig. 5b with asterisk represents 93% switching at a pulse width of 67 ps.

In summary, higher DMI can result in formation of skyrmions in smaller nanodots at low M_s but such high values of DMI have not yet been experimentally observed. To create skyrmions in confined structures ~ 20 nm lateral dimensions with experimentally observed DMI ~ 3 mJ/m^2, one needs large demagnetization (stray field) from materials that can be achieved with a high M_s. We also showed that using a material with high saturation magnetization can help achieve thermally robust and extremely energy efficient switching in 20 nm ferromagnetic nanodot with experimentally demonstrated DMI. Thus, use of materials with high M_s can provide a pathway for aggressive scaling of ferromagnetic skyrmion mediated VCMA switching of p-MTJs with lateral dimensions ~ 20 nm and beyond.

Method

The magnetization dynamics of circular nanodots was simulated by using the micromagnetic simulation software Mumax3[33] for 50 nm, 30 nm and 20 nm lateral dimensions with a constant cell size of $0.5 \times 0.5 \times 0.6$ nm^3. In the Mumax3 framework, the magnetization dynamics is simulated by solving the Landau–Lifshitz–Gilbert (LLG) equation:

$$\frac{\partial \vec{m}}{\partial t} = \left(\frac{-\gamma}{1+\alpha^2}\right)\left[\vec{m} \times \vec{B}_{eff} + \alpha\left\{\vec{m} \times \left(\vec{m} \times \vec{B}_{eff}\right)\right\}\right] \tag{1}$$

where α is the Gilbert damping coefficient and γ is the gyromagnetic ratio (rad/Ts). $\vec{m}$ is the normalized magnetization vector ($\vec{M}/M_s$), M_s is the saturation magnetization and $\vec{B}_{eff}$ is the effective magnetic field having the following components[33]:

$$\vec{B}_{eff} = \vec{B}_{demag} + \vec{B}_{exchange} + \vec{B}_{dm} + \vec{B}_{anis} + \vec{B}_{thermal} \tag{2}$$

Here, $\vec{B}_{demag}$ is the effective field due to demagnetization energy and $\vec{B}_{exchange}$ is the Heisenberg exchange interaction.

$\vec{B}_{dm}$ yields the Dzyaloshinskii–Moriya interaction:

$$\vec{B}_{dm} = \frac{2D}{M_s}\left(\frac{\partial m_z}{\partial x}, \frac{\partial m_z}{\partial y}, -\frac{\partial m_x}{\partial x} - \frac{\partial m_y}{\partial y}\right) \tag{3}$$

where m_x, m_y and m_z are the normalized magnetization components along the three cartesian co-ordinates and D represents the DMI constant (J/m^2).

$\vec{B}_{anis}$, the effective field due to perpendicular anisotropy, is given by the following equation:

$$\vec{B}_{anis} = \frac{2K_{u1}}{M_s}(\vec{u}.\vec{m})\vec{u} \tag{4}$$

Here K_{u1} indicates first order uniaxial anisotropy constant and $\vec{u}$ stands for a unit vector in the anisotropy direction. The temperature effect is calculated by:

$$\vec{B}_{thermal} = \vec{\eta}(step)\sqrt{\frac{2\alpha k_B T}{M_s \gamma \Delta V \Delta t}} \tag{5}$$

where T is the temperature (K), ΔV is the cell volume, k_B is the Boltzmann constant, Δt is time step and $\vec{\eta}(step)$ is a random vector from a standard normal distribution which is independent (uncorrelated) for each of the three cartesian co-ordinates. Its value is changed after every time step.

The parameters listed in Table 1 were used for all of the simulation cases unless otherwise stated.

Received: 26 August 2021; Accepted: 30 September 2021
Published online: 22 October 2021

References

1. Fert, A., Cros, V. & Sampaio, J. Skyrmions on the track. *Nature Nanotechnol.* **8**(3), 152–156 (2013).
2. Zhang, X. *et al.* Skyrmion-electronics: Writing, deleting, reading and processing magnetic skyrmions toward spintronic applications. *J. Phys. Condens. Matter* **32**(14), 143001 (2020).
3. Tomasello, R. *et al.* A strategy for the design of skyrmion racetrack memories. *Sci. Rep.* **4**(1), 6784 (2014).
4. Iwasaki, J., Mochizuki, M. & Nagaosa, N. Universal current-velocity relation of skyrmion motion in chiral magnets. *Nat. Commun.* **4**, 1463 (2013).
5. Everschor, K., Garst, M., Duine, R. A. & Rosch, A. Current-induced rotational torques in the skyrmion lattice phase of chiral magnets. *Phys. Rev. B* **84**, 064401 (2011).
6. Iwasaki, J., Mochizuki, M. & Nagaosa, N. Current-induced skyrmion dynamics in constricted geometries. *Nat. Nanotechnol.* **8**, 742–747 (2013).
7. Nagaosa, N. & Tokura, Y. Topological properties and dynamics of magnetic skyrmions. *Nat. Nanotechnol.* **8**, 899–911 (2013).
8. Yu, X. Z. *et al.* Skyrmion flow near room temperature in an ultralow current density. *Nat. Commun.* **3**, 988 (2012).
9. Jiang, W. *et al.* Direct observation of the skyrmion Hall effect. *Nat. Phys.* **13**, 162–169 (2016).
10. Woo, S. *et al.* Current-driven dynamics and inhibition of the skyrmion Hall effect of ferrimagnetic skyrmions in GdFeCo films. *Nat. Commun.* **9**, 959 (2018).
11. Kasai, S., Sugimoto, S., Nakatani, Y., Ishikawa, R. & Takahashi, Y. K. Voltage-controlled magnetic skyrmions in magnetic tunnel junctions. *Appl. Phys. Express* **12**, 083001 (2019).
12. Bhattacharya, D., Al-Rashid, M. M. & Atulasimha, J. Voltage controlled core reversal of fixed magnetic skyrmions without a magnetic field. *Sci. Rep.* **6**, 31272 (2016).
13. Bhattacharya, D. & Atulasimha, J. Skyrmion-mediated voltage-controlled switching of ferromagnets for reliable and energy-efficient two-terminal memory. *ACS Appl. Mater. Interface* **10**(20), 17455–17462 (2018).
14. Bhattacharya, D. *et al.* Creation and annihilation of non-volatile fixed magnetic skyrmions using voltage control of magnetic anisotropy. *Nat. Electron.* **3**, 539–545 (2020).
15. Rajib, M. M., Misba, W. A., Bhattacharya, D., Garcia-Sanchez, F. & Atulasimha, J. Dynamic skyrmion-mediated switching of perpendicular MTJs: Feasibility analysis of scaling to 20nm with thermal noise. *IEEE Trans. Electron Devices* **67**, 9 (2020).
16. Grezes, C. *et al.* Ultra-low switching energy and scaling in electric-field-controlled nanoscale magnetic tunnel junctions with high resistance-area product. *Appl. Phys. Lett.* **108**, 012403 (2016).
17. Moreau-Luchaire, C. *et al.* Additive interfacial chiral interaction in multilayers for stabilization of small individual skyrmions at room temperature. *Nat. Nanotech.* **11**, 444–448 (2016).
18. Soumyanarayanan, A. *et al.* Tunable room-temperature magnetic skyrmions in Ir/Fe/Co/Pt multilayers. *Nat. Mater.* **16**, 898–904 (2017).
19. Woo, S. *et al.* Observation of room-temperature magnetic skyrmions and their current-driven dynamics in ultrathin metallic ferromagnets. *Nat. Mater.* **15**, 501–506 (2016).
20. Tolley, R., Montoya, S. A. & Fullerton, E. E. Room-temperature observation and current control of skyrmions in Pt/Co/Os/Pt thin films. *Phys. Rev. Mater.* **2**, 044404 (2018).
21. Buttner, F., Lemesh, I. & Beach, G. S. D. Theory of isolated magnetic skyrmions: From fundamentals to room temperature applications. *Sci. Rep.* **8**, 4464 (2018).
22. Du, H. *et al.* Edge-mediated skyrmion chain and its collective dynamics in a confined geometry. *Nat Commun* **6**, 8504 (2015).
23. Jin, C. *et al.* Control of morphology and formation of highly geometrically confined magnetic skyrmions. *Nat Commun* **8**, 15569 (2017).
24. Sisodia, N. & Muduli, P. K. Thermal decay of a single Neel skyrmion via helicity slip in a nanodisks. *Phys. Status Solidi RRL* **14**, 1900525 (2019).
25. Boulle, O. *et al.* Room-temperature chiral magnetic skyrmions in ultrathin magnetic nanostructures. *Nat. Nanotechnol.* **11**, 449–454 (2016).
26. Sampaio, J., Cros, V., Rohart, S., Thiaville, A. & Fert, A. Nucleation, stability and current-induced motion of isolated magnetic skyrmions in nanostructures. *Nat. Nanotechnol.* **8**, 839–844 (2013).
27. Zhang, X. *et al.* Skyrmions in magnetic tunnel junctions. *ACS Appl. Mater. Interfaces.* **10**(19), 16887–16892 (2018).
28. Cao, A. *et al.* Enhanced interfacial Dzyaloshinskii–Moriya interactions in annealed Pt/Co/MgO structures. *Nanotechnology* **31**(15), 155705 (2020).
29. Caretta, L. *et al.* Fast current-driven domain walls and small skyrmions in a compensated ferrimagnet. *Nat. Nanotechnol.* **13**(12), 1154–1160 (2018).
30. Ma, C. T., Xie, Y., Sheng, H., Ghosh, A. W. & Poon, S. J. Robust formation of ultrasmall room-temperature Neel skyrmions in amorphous ferrimagnets from atomistic simulation. *Sci. Rep.* **9**, 9964 (2019).
31. Danan, H., Herr, A. & Meyer, A. J. P. New determinations of the saturation magnetization of Nickel and Iron. *J. Appl. Phys.* **39**, 669 (1968).
32. Evans, R. F. L. *et al.* Atomistic spin model simulations of magnetic nanomaterials. *J. Phys. Condens. Matter* **26**(10), 103202 (2014).
33. Vansteenkiste, A. *et al.* The design and verification of MuMax3. *AIP Adv.* **4**(10), 107133 (2014).
34. Nozaki, T. *et al.* Highly efficient voltage control of spin and enhanced interfacial perpendicular magnetic anisotropy in iridium-doped Fe/MgO magnetic tunnel junctions. *NPG Asia Mater* **9**, e451 (2017).
35. Cheng, H. *et al.* Giant perpendicular magnetic anisotropy in Mo-based double-interface free layer structure for advanced magnetic tunnel junctions. *Adv. Electron. Mater.* **6**, 1–8 (2020).
36. Kato, Y. *et al.* Giant voltage-controlled magnetic anisotropy effect in a crystallographically strained CoFe system. *Appl. Phys. Express* **11**(5), 053007 (2018).
37. Munira, K. *et al.* Reducing error rates in spintronic multiferroic nanomagnetic logic by pulse shaping. *Nanotechnology* **26**(24), 245202 (2015).
38. Nguyen, T. N. A. *et al.* [Co/Pd]–NiFe exchange springs with tunable magnetization tilt angle. *Appl. Phys. Lett.* **98**, 172502 (2011).
39. Kampen, M. V. *et al.* All-optical probe of coherent spin waves. *Phys. Rev. Lett.* **88**, 227201 (2002).

Acknowledgements

M. M. R., D. B. and J. A. were supported by the National Science Foundation (NSF) Software and Hardware Foundations (SHF) Small Grant 1909030.

Author contributions

M. M. R. performed the simulations. All authors contributed to conceiving the idea and writing the paper.

Competing interests

The authors declare no competing interests.

Additional information

Supplementary Information The online version contains supplementary material available at https://doi.org/10.1038/s41598-021-99780-1.

Correspondence and requests for materials should be addressed to J.A.

Reprints and permissions information is available at www.nature.com/reprints.

Publisher's note Springer Nature remains neutral with regard to jurisdictional claims in published maps and institutional affiliations.